Supporting Information

Blinder et al. 10.1073/pnas.1007239107

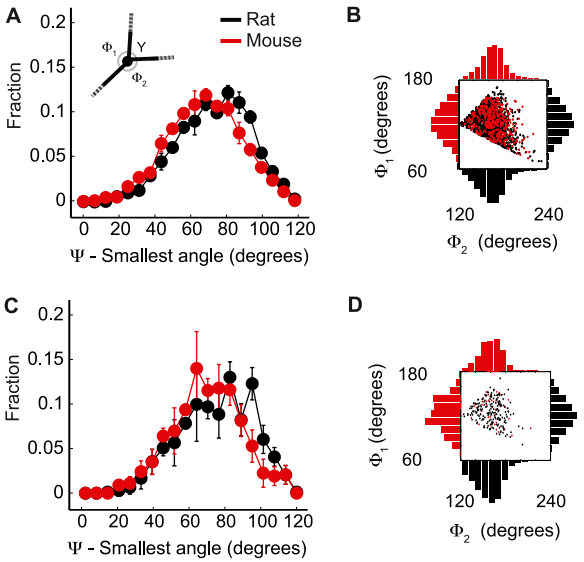

Fig. S1. Angles between edges connected to branching vertices. The branching angles for vertices with coordination number of 3 are analyzed in terms of the distribution of the smallest angle, denoted Ψ, and the symmetry between the remaining two angles, denoted Φ_1 and Φ_2. (*A*) The distribution of the smaller branching angle, Ψ, for all vertices shows a difference of 5° in mean value between rats and mice ($P < 0.01$, KS-test). (*B*) Evidence for a slight asymmetry between the larger branch angles, as seen by a skewed histogram for the largest angle, for both rats and mice. (*C* and *D*) The branching angles, as in *A* and *B*, for backbone vertices only.

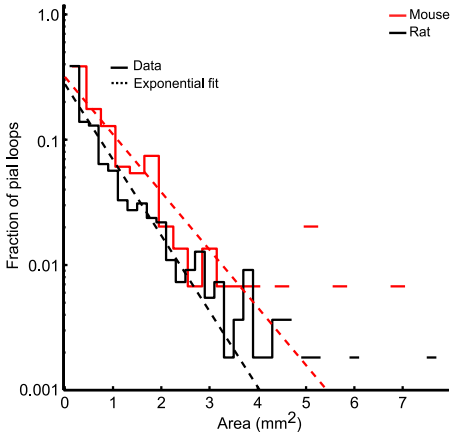

Fig. S2. Distribution of the area of loops in the backbone. The area of the loops is fit with an exponential function with mean values of 0.94 ± 0.14 mm^2 (mean ± 95% confidence interval) and 0.72 ± 0.06 mm^2 for rat and mice, respectively. Shown on semilogarithmic plot.

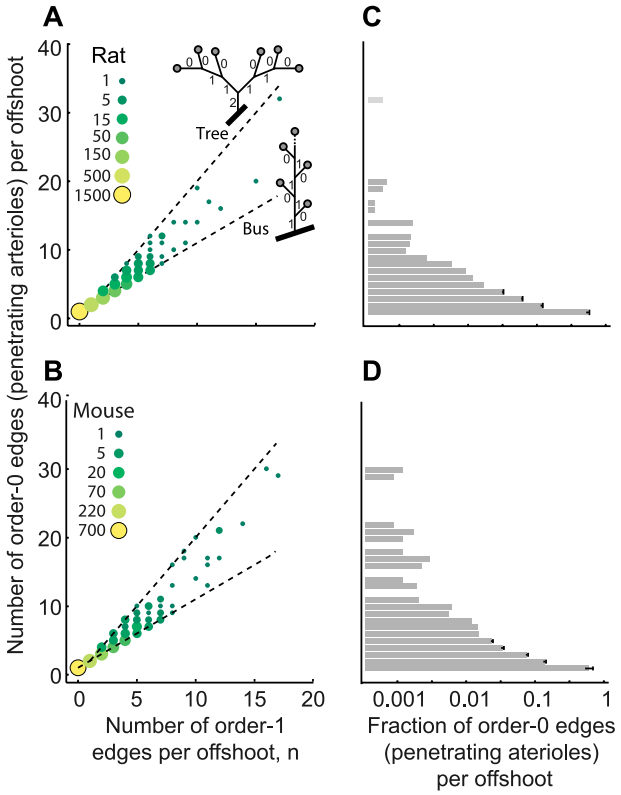

Fig. S3. Penetrating arterioles branch from the backbone. (*A* and *B*) The small fraction of ramified offshoot branches tend to have a more pronounced "bus-like" branching pattern (n = 5,678 and 3,477 rat and mouse edges, repectively, grouped in the previously mentioned offshoots); note the logarithmic bubble scale. (*C* and *D*) Penetrating arterioles vertices within the subgraphs of *A* and *B*, respectively.

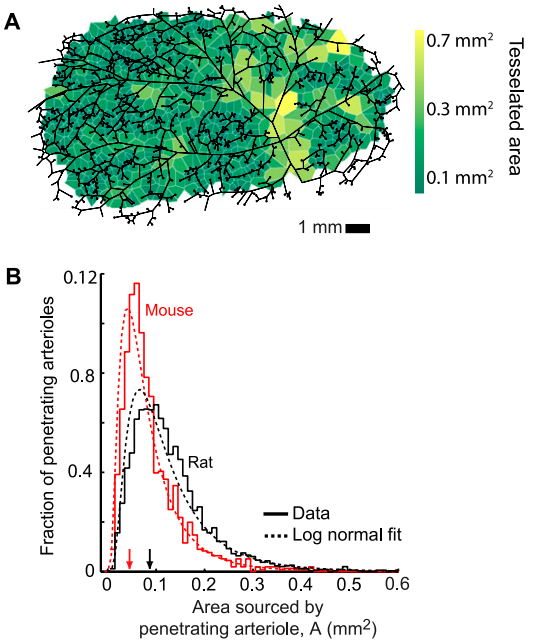

Fig. S4. Penetrating arterioles serve uneven areas across the cortex. The territory served by each penetrating arteriole was estimated by tessellation of maps. (*A*) Example of a rat middle cerebral artery (MCA) and its estimated tessellation of the pial surface (yellow-green polygons). Tessellation was computed based on ultimate dilation algorithm seeded at the location of penetrating arteries. Areas with higher penetrating arteriole density result in smaller territories and vice versa. Penetrating arteriole territories next to the perimeter of the MCAs were omitted from the analysis to exclude erroneous area estimations because of edge effects in the tessellation analysis. The tessellation process also reveals that the largest territories are found along the corridor of the major MCA trunk, and smaller territories are observed in medial areas. (*B*) Mice and rat share similar distributions for the tessellation areas of their penetrating arterioles, with a significant shift to smaller areas in mice cortex (KS-test, $P < 0.001$, $n = 3{,}450$ and 1,945 penetrating arterioles for rat and mice, respectively). Both distributions may be fit by a log-normal density functions (dashed lines), with mean and variance ($\pm$ 95% confidence intervals) of 0.09 ± 0.005 and 0.005 ± 0.001 for mouse and 0.13 ± 0.004 and 0.009 ± 0.001 for rat, respectively. The distributions of areas for these territories peaks near 0.06 and 0.10 mm^2 for mouse and rat, respectively, corresponding to diameters of 250 and 350 μm for the cross-section of equivalent cylinders; the latter value coincides with that in the occlusion experiments (Fig. 5).

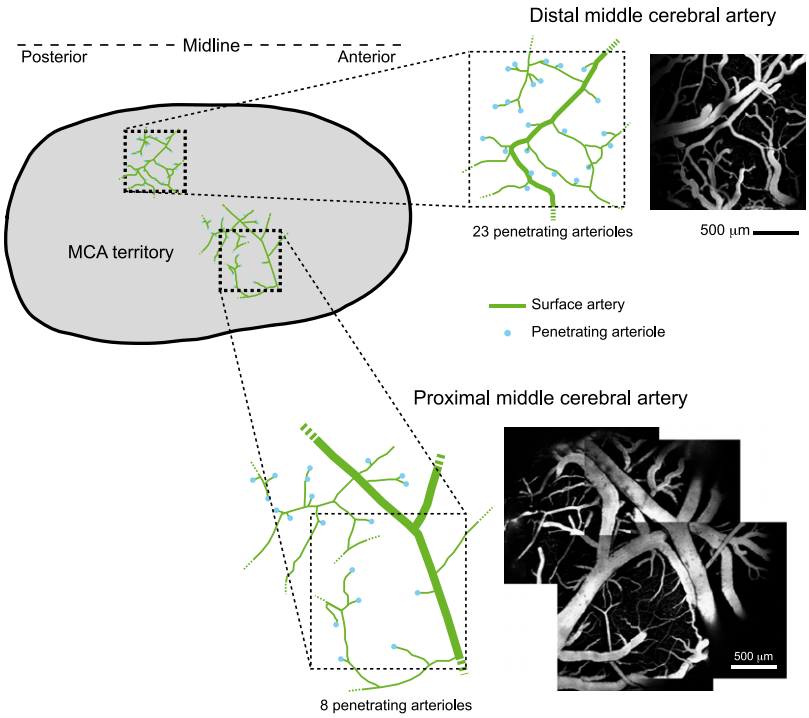

Fig. S5. Penetrating arteriole density is greater in distal versus proximal territories of the MCA. In two separate rats, cranial windows were generated over the somatosensory cortex to image the distal MCA or over the piriform cortex to image the proximal MCA branches. Two-photon imaging was used to define the location of all penetrating arterioles within the field, to verify the group results obtained by wide-field fluorescence microscopy on flattened cortices. In the proximal MCA case, an arteriole branch traversed beneath a large vein that was too absorbing to image through, possibly leading to an underestimation of one or two penetrating arterioles at most. Nevertheless, an ~3-fold greater density in clearly observed in distal versus proximal regions of the MCA.

Table S1. Flow parameters in low-flux versus high-flux penetrating arterioles

	Pre-occlusion			Post-occlusion		
	Diameter (mean ± SD) μm	Speed (mean ± SD) mm/s	Flux (mean ± SD) nL/s	Diameter (mean ± SD) μm	Speed (mean ± SD) mm/s	Flux (mean ± SD) nL/s
Low	10 ± 1	5.3 ± 0.4	0.21 ± 0.03	12 ± 1	4.7 ± 0.7	0.24 ± 0.03
High	21 ± 2	7.7 ± 0.7	1.4 ± 0.2	23 ± 4	4.5 ± 1.0*	0.6 ± 0.1*
Ctrl	16 ± 2	6.1 ± 1.1	0.8 ± 0.1	17 ± 1	6.0 ± 0.6	0.8 ± 0.1

*Change from pre-occlusion values is significant ($p < 0.05$, Wilcoxon test).

Table S2. Physiological parameters for *in vivo* blood flow studies

	Pre-occlusion	Post-occlusion
MABP* (mmHg)	89 ± 3	89 ± 2
PaO_2 (mmHg)	118 ± 6	121 ± 4
$PaCO_2$ (mmHg)	30 ± 1	30 ± 1
pH	7.36 ± 0.01	7.36 ± 0.01

*mean arterial blood pressure.